Tailor-made directional emission in nanoimprinted plasmonic-based light-emitting devices

Gabriel Lozano, Grzegorz Grzela, Marc A. Verschuuren, and Jaime Gómez Rivas*

Dr. G. Lozano, Dr. Grzegorz Grzela and Prof. Jaime Gómez Rivas
Center for Nanophotonics, FOM Institute AMOLF
c/o Philips Research, High-Tech Campus 4, NL-5656AE, Eindhoven, The Netherlands

Dr. G. Lozano
Present address: Instituto de Ciencia de Materiales de Sevilla, Consejo Superior de
Investigaciones Científicas-Universidad de Sevilla (CSIC-US)
Américo Vespucio 49, 41092 Sevilla, Spain.
E-mail: g.lozano@csic.es

Dr. M. A. Verschuuren
Philips Research
High-Tech Campus 4, NL-5656AE, Eindhoven, The Netherlands

Prof. Jaime Gómez Rivas
COBRA Research Institute, Eindhoven University of Technology
P.O. Box 513, NL-5600MB Eindhoven, The Netherlands

Efficient energy generation and management is a global concern nowadays.[1-3] Artificial

lighting represents a significant fraction of all electrical energy consumed worldwide. With

the advent of very efficient light sources based on light-emitting diodes (LEDs), solid-state

lighting (SSL) technology is gradually prevailing upon traditional light sources due to the

higher efficiencies and longer lifetimes of the emerging SSL devices.[4-8] In order to achieve

white-light using LEDs,[9] frequency down-conversion of blue light from InGaN-based LEDs

by suitable wavelength or color-converters has become a dominant technique.[10-12] The color-

converting material is a highly efficient and stable luminescent layer made of rare earth ions,

dye molecules or quantum dots, which typically shows a Lambertian emission.[13]

Consequently, the angular distribution of light emission in a SSL device is difficult to

1

shape.[14-18] The fundamental research in SSL is now shifting towards the use of nanostructures, with the aim of a precise control over the light extraction of blue LEDs,[19] the brightness, the directionality and the spectrum of color-converting materials.[20] Nanostructuring strategies represent a versatile approach to tailor the emission properties of the color-converting layer without changing the material structure or the chemical composition of efficient color-converters. The field of plasmonics offers a route to control light-matter interaction in the nanoscale with high accuracy through the use of strong local field enhancements near metal nanostructures.[21,22] It has been found that the emission characteristics of light sources located in the proximity of metal nanoparticles can be strongly modified.[23-31] While individual metal nanoparticles sustain localized surface plasmon polaritons (LSPPs), an array of such particles can also support delocalized plasmonic-photonic hybrid states due to the coupling of LSPPs to diffracted or refractive-index guided modes.[32] Diffractive and waveguide coupling give rise to collective lattice-induced modes (LMs) known as surface lattice resonances[33] and waveguide-plasmon polaritons,[34] respectively. These resonances are responsible for large field enhancements that extend away from the nanoparticles in the volume in which the wavelength-converting material is distributed.[35-41] Several experimental works have addressed the emission of quantum emitters in the proximity of the LMs. These include the directional out coupling of the emission through dipolar and multipolar resonances,[42,43] the strong coupling of excitons to LMs,[44,45] and lasing.[46] In turn, a tailor-made control over the directionality of light-emitting devices has not yet been realized.

In this communication, we demonstrate that the emission directionality of color-converting LEDs can be accurately controlled using periodic arrays of metal nanoparticles arranged in a hexagonal lattice. The hexagonal lattice or equilateral triangular lattice is one of the five Bravais bi-dimensional lattices. It shows six-fold symmetry that facilitates a nearly homogeneous distribution of the emission over the azimuthal angle. The color converter

consists of a polymer layer doped with a highly efficient dye deposited over an array of Al nanoparticles. The metal nanostructures are fabricated using a Nanoimprint Lithography (NIL) technique in combination with a reactive ion etching (RIE) process. NIL is a simple nanofabrication method that has attracted a lot of attention in several fields of research for different applications due to its high resolution and large throughput.[47-49] A high power blue LED is employed to excite the emitting material. The directionality of the resulting emission of the device is investigated using Fourier microscopy (FM). Excited dye molecules dispersed in the color-converting layer deposited over the array can couple to LMs, which radiate into free space. The coherent scattering from periodically arranged metal nanoparticles enables the beaming of most of the emission into small solid angles in defined directions. Here we demonstrate that by tailoring the lattice constant of the array, and consequently the onset of diffraction, it is possible to increase the emission intensity in defined directions and shape the directionality of the color-converting LEDs using plasmonics. We will show that metal nanostructure arrays act as diffractive nano optics to accurately control the angular distribution of light-emitting devices.

NIL makes use of nanostructured stamps to mold a resist layer into a three-dimensional shape, thereby transferring a nanostructure from the stamp into the resist. Substrate conformal imprint lithography (SCIL) is a novel NIL technique that uses composite stamps where the nanostructure is in a silicone rubber which is grafted on a 200 μm-thin glass sheet.[50] This allows the faithful replication of nanopatterns over large-area substrates, i.e. up to 20 cm in diameter. Replicated patterns with details smaller than 10 nm have been demonstrated using NIL.[51,52] **Figure 1** (a) illustrates the fabrication process of a plasmonic-based color-converting layer, i.e. a dye-doped polymer layer that covers a periodic array of Al nanoparticles deposited on a glass silica substrate. Al is chosen as metal because it exhibits a plasmonic behavior in the blue part of the electromagnetic spectrum, is inexpensive and easy to process. The dye is stable, bright in the red part of the spectrum where the human eye is

most sensitive and shows a close-to-one photoluminescence quantum yield, all of which make it highly suitable for SSL applications. Figure 1 (b-e) shows scanning electron microscope pictures of a top view of the nanoimprinted Al arrays, which are characterized by a lattice constant of a=325 nm, a=375 nm, a=425 nm and a=475 nm, respectively.

In order to investigate the angular emission of the light-emitting device, FM is employed. Images of the intensity distribution on the back focal plane (BFP, so-called Fourier plane) of a high numerical aperture (NA) objective are recorded on a charge-coupled device (CCD) camera.[53] Fourier images contain information about the intensity of light emitted in different directions from the normal to the substrate. **Figure 2** shows a sketch of the light-emitting device and a ray tracing diagram for three different emission angles: θ_1, θ_2 and θ_3, to illustrate the principle of FM. Every plane wave emitted from the object plane reaches the same point at the BFP. In particular, light emitted at an angle θ_1 (θ_2) is collected at a distance x_1 (x_2) from the center of the Fourier image, wherein light emitted into the normal direction from the sample is detected. The NA of the objective determines the largest angle that can be picked up by the objective according to θ_{max}=arcsin(NA). Thus, light emitted with an angle $\theta_3 > \theta_{max}$ will not reach the BFP nor the detector. FM enables a fast and accurate quantitative characterization of the directionality of the emission of SSL devices.

An electrically driven high-power blue LED (λ_{ex}=445 ± 15 nm) is employed to optically pump the color-converter now featuring a nanoparticle array. The emission originated in the color-converting layer is collected in the Fourier plane. No polarization selection is carried out since polarization dependency is generally unwanted in SSL systems. The Fourier images are plotted in polar coordinates, where the radius represents the elevation angle of emission (θ) and the polar angle corresponds to the azimuthal angle of emission (ϕ) –see the inset in **Figure 3**-. The large NA of the microscope objective (0.95) allows collecting large angles of emission limited by θ_{max}=72 deg. from the normal to the sample. Figure 3 (a) displays the

4

Fourier image of the unpolarized emission (in units of counts per 0.1 s) from the color-converting layer deposited over a flat dielectric substrate that will be considered as the reference color-converting LED. A 10 nm band-pass filter is employed to spectrally select the emission at λ=620 nm, where the emission spectrum of the dye peaks. The emission pattern shows no particular directional features. This is expected for a random distribution of dye molecules deposited over a flat surface, which behaves as a Lambertian source. The emission of such layer deposited over hexagonal arrays with lattice constant a=475 nm, a=425 nm and a=375 nm is shown in Figure 3 (b), 3 (c) and 3 (d), respectively. The emission is collected in the same spectral range used for the reference measurement (λ=615-625 nm). The effect of the combination of periodic arrays of metal nanoparticles with a color-converting layer is twofold: (i) an enhancement of the amount of light extracted from the emitting layer and (ii) a drastic modification of the angular distribution of the emission. Fourier images reveal a strong directional response of the emission with bands of bright luminescence that are associated to lattice-induced modes. These features depend on the separation between metal nanoparticles in the array. Clear six fold symmetry is observed due to the geometry of the hexagonal lattice. The higher symmetry of the hexagonal lattice, compared to the most widely employed square lattice, is beneficial for SSL since it provides a more even distribution of the light emission over the azimuthal angle. In order to gain more physical insight on the different emission patterns attained for the arrays with different interparticle distances, we calculate the onset of diffraction or the Rayleigh anomalies (RAs) for the different diffracted orders supported by the investigated lattices. Figure 3 (e), 3 (f) and 3 (g) show the RAs calculated for the ($\pm$1,0), (0, $\pm$1), (-1,1) and (1,-1) orders diffracted by a hexagonal array with lattice constant a=475 nm, a=425 nm and a=375 nm, respectively, at λ=620 nm in a medium with a refractive index of 1.46. The coupling of the light emitted by the dye molecules distributed in the color-converting layer to lattice-induced modes supported by the array gives rise to narrow bands of

5

enhanced directional emission that follow the dispersion of the RAs. We note that the experimental emission consists of double nearly parallel bands -clearly seen in Figure 3(d)-. These double bands have been reported in Reference [29] and can be attributed to the excitation of lattice resonances induced by in-plane scattering and waveguide-plasmon polaritons in the dye layer.

A periodic array of metal nanoparticles behaves as a phased array of optical antennas in which the radiation pattern of sub-wavelength sources is modified by the coherent scattering of the periodically spaced metallic nanoparticles. Light coupled out by the array interferes constructively in defined directions, resulting in an efficient beaming of the light emitted by the color-converting layer. The beaming of the emission can be also interpreted in terms of the increased spatial coherence of point sources due to their coupling to the extended LMs. To assess the directionality of the emission by the arrays, the emitted intensity collected in the Fourier images shown in Figure 3 (a-d) is integrated over the azimuthal coordinate (ϕ).

Figure 4 (a) displays the polar plots of the azimuthally integrated emitted intensity in which each curve is normalized to its maximum. It is observed that the beaming angle, that is the direction along which most of the light is emitted, can be accurately controlled by tailoring the interparticle distance in the periodic array. Specifically, the beaming angle increases as the lattice constant of the array decreases. The emission spectrum of the color-converting layer overlaps with the LM at a larger angle when the separation between particles in the array diminishes. For comparison, the gray filled area in Figure 4 (a) is a polar plot of the azimuthally integrated Fourier image presented in Figure 3 (a), which displays the emission of the color-converting layer deposited over a flat glass substrate. A careful inspection of this curve shows a small modulation of the intensity, which is an artifact that originates from the imaging system in the experimental setup. Figure 4 (b) displays the beaming angle measured as a function of the lattice parameter for different arrays (black squares). The RA of the (1,0) diffracted beam calculated at λ=620 nm as a function of the lattice constant and the elevation

angle (θ) for ϕ=0 deg is also shown as a dashed curve in the same plot. The shift of the measurements with respect to the RA is the result of the coupling of RAs with LSPPs which gives rise to the LMs to which the emission of the dye couples.[54] This analysis reveals that an accurate control of the periodicity of the array allows tailoring the directionality of the emission of plasmonic-based LEDs.

To further elucidate the modification of the spontaneous emission intensity, in Figure 4 (c) we plot the photoluminescence directional enhancement (PLDE), i.e., the emission intensity of the plasmonic color converter at the beaming angle normalized by the emission of the color converter at the same angle in the absence of nanoparticles, as a function of the lattice parameter of the hexagonal array. In general, the PLDE can be factorized into two contributions assuming that the excitation and the emission are two independent processes occurring at different wavelengths (λ_{ex} and λ, respectively).[55,42] Thus, the PLDE can be expressed as

$$PLDE(\lambda_{ex},\Omega_{ex},\lambda,\Omega) = \frac{\int_V \eta(\vec{r},\lambda,\Omega)\left|E(\vec{r},\lambda_{ex},\Omega_{ex})\right|^2 dV}{\int_V \eta_{ref}(\vec{r},\lambda,\Omega)\left|E_{ref}(\vec{r},\lambda_{ex},\Omega_{ex})\right|^2 dV} \qquad (1)$$

where V is the volume of the color-converting layer. Ω_{ex} is the solid angle associated to the elevation and the azimuthal angle of excitation, $E(\vec{r},\lambda_{ex},\Omega_{ex})$ is the local field at the wavelength λ_{ex} and at the position $\vec{r}$ where each dye molecule is located. $E_{ref}(\vec{r},\lambda_{ex},\Omega_{ex})$ corresponds to the local field in the absence of the hexagonal array. The term $\eta(\vec{r},\lambda,\Omega)$ includes the effect of the modified local density of optical states at $\vec{r}$ to which a dye molecule can decay due to the presence of the hexagonal array and; the out coupling of this emission to free space radiation in the solid angle Ω. $\eta_{ref}(\vec{r},\lambda,\Omega)$ represents the same physical quantity than $\eta(\vec{r},\lambda,\Omega)$, but in the absence of the array. The geometry of the device is such that the color-converting layer is mainly illuminated along the normal direction to the array. We have

7

performed 3D numerical simulations (not shown here) in order to elucidate the influence of

the excitation enhancement contribution, given by $\dfrac{\int_V \left| E\left(\vec{r}, \lambda_{ex}, \Omega_{ex}\right)\right|^2 dV}{\int_V \left| E_{ref}\left(\vec{r}, \lambda_{ex}, \Omega_{ex}\right)\right|^2 dV}$. The calculations

reveal that this contribution is approximately 4-fold when the lattice parameter is 325 nm. For

this interparticle distance, the blue LED light couples very efficiently to LMs supported by the

array at λ_{ex}, leading to the largest PLDE (12-fold). For the other lattices, in which the effect

of the excitation enhancement is negligible, the PLDE is ~3.5-fold. We attribute most of this

overall enhancement to an improved out coupling of the emission from the color-converting

layer. The metallic nanoparticle array acts as an efficient scattering layer that facilitates light

extraction from the dye-doped polymer layer, preventing light guiding in the substrate.

In conclusion, using Fourier Microscopy we have shown that large-area nanoimprinted

hexagonal plasmonic lattices strongly shape the directionality of the emission of light-

emitting devices. By controlling the separation between metal nanoparticles in the array, we

have demonstrated an enhanced directional emission from a random distribution of dye

molecules. These molecules emit with a close-to-one PL quantum yield in the red part of the

visible spectrum where the human eye is most sensitive. We envisage that the use of

nanoimprinted metallic arrays will provide a wealth of new opportunities for the design and

optimization of solid-state lighting devices in which the control over directionality and color

plays a major role.

Experimental Section

Nanofabrication: Our samples consist of a polystyrene layer doped with dye molecules

deposited over an array of Al nanoparticles fabricated on glass substrates. The substrates are

first cleaned with a mixture of H_2SO_4 and H_2O_2, UV-ozone and thoroughly rinsed using

demineralized water. Then, a 30 nm layer of Al_2O_3 is deposited by sputtering, after which a

150 nm-thick layer of Al is deposited using the same method. Before nanoimprinting, the Al

samples are cleaned with oxygen plasma. Then, a ca. 60 nm-thick sol-gel resist is applied by

spin-coating. Shortly after the spin-coating cycle is finished, the SCIL stamp is applied into the resist. The stamp consists of several hexagonal arrays of holes in which the interparticle distance ranges from 300 nm to 475 nm in steps of 25 nm. The sol-gel was cured by applying 365 nm UV light on the stamp. Next the stamp is carefully released and the sample is given a post bake at 150°C. This results in silica sol-gel nanoparticles of 80 nm to 150 nm in diameter and ca. 100 nm in height on top of the Al layer. The nanoimprinted sol-gel patterns are subsequently transferred into the Al by a RIE technique. First the residual layer beneath the sol-gel particles is removed using CF_4/N_2. Approximately 55 nm of sol-gel is removed, which ensures that the areas between the sol-gel nanoparticles are clear of resist and the Al is exposed. The sample is then transferred under vacuum to a second RIE chamber, which uses Cl_2 and BCl_3 to etch, and N_2 and CH_4 to passivate. The combination of NIL and RIE allows a high-throughput patterning of large-area nanoplasmonic structures with great precision and at low costs. Finally, over the Al nanoparticle arrays, a 700 nm-thick polystyrene layer doped with dye molecules (BASF, Lumogen F Red 305) at 3% of mass fraction, which acts as a color-converting layer, is deposited by spin coating. The fabricated samples are finally placed in optical contact with a high-power blue LED (λ_{ex}=445±15 nm) module that is used to excite the color-converter.

Optical measurements: Fourier images are taken using a setup based on an optical microscope (Leica, DMLM/P). The light-emitting device is mounted on a computer-controlled 3-axis piezo stage (Melles Griot, NanoMax). The blue LED is electrically driven and the emission from the device is collected using a microscope objective (Leica, HCX PL APO 100x) with NA = 0.95. In order to measure the emission pattern, an achromatic lens is used to image the BFP of the objective on a CCD camera (Andor Luca-S). The wavelength range is selected using a band pass filter (λ=620±5 nm).

Numerical simulations. Full-wave calculations of the spatial distribution of the electric field intensity at the excitation wavelength are obtained using FDTD Solutions (Lumerical

Solutions Inc). In order to calculate the spatial distribution of the local electric field intensity, a simulation box of a unit cell of the hexagonal array containing two nanoparticles, with perfectly matched layer in the z direction and periodic boundary conditions in the in-plane directions were used. A three-dimensional frequency-domain field monitor and a three-dimensional refractive index monitor that contain both the layer of refractive index 1.59 and the metallic nanoparticles were employed. The optical constants of Al were taken from Reference [56].

[1]   B. O'Regan, M Gratzel, *Nature* **1991**, *353*, 737.

[2]   E. F. Schubert, J. K. Kim, *Science* **2005**, *308*, 1274.

[3]   A. S. Aricò, P. Bruce, B. Scrosati, J.-M. Tarascon, W. van Schalkwijk, *Nat. Mater.* **2005**, *4*, 366.

[4]   A. Zukauskas, M. S. Shur, R. Caska, *Introduction to Solid-state Lighting*, John Wiley & Sons **2002**.

[5]   D. A. Steigerwald, J. C. Bhat, D. Collins, R. M. Fletcher, M. O. Holcomb, M. J. Ludowise, P. S. Martin, S. L. Rudaz, *IEEE J. Sel. Top. Quantum Electron.* **2002**, *8*, 310.

[6]   J. Y. Tsao, "Solid-state lighting: lamps, chips, and materials for tomorrow", IEEE Circuits & Devices **2004**, *20*, 28.

[7]   B. W. D'Andrade, S. R. Forrest, *Adv. Mater.* **2004**, *16*, 585.

[8]   J. M. Phillips, M. E. Coltrin, M. H. Crawford, A. J. Fischer, M. R. Krames, R. M. Mach, G. O. Mueller, Y. Ohno, L. E. S. Rohwer, J. A. Simmons, J. Y. Tsao, *Laser & Photon. Rev.* **2007**, *1*, 307.

[9]   P. Schlotter, R. Schmidt, J. Schneider, *Appl. Phys., A Mater. Sci. Process.* **1997**, *64*, 417.

[10]   N. C. Hu, C. C. Wu, S. F. Chen, H. C. Hsiao, *Appl. Opt.* **2008**, *47*, 3423.

[11]   R. Mueller-Mach, G. O. Mueller, M. R. Krames, O. B. Shchekin, P. J. Schmidt, H. Bechtel, C.-H. Chen, O. Steigelmann, *Phys. Status Solidi RRL* **2009**, *3*, 215.

[12]   S. Pimputkar, J. S. Speck, S. P. Den Baars, S. Nakamura, *Nat. Photon.* **2009**, *3*, 180.

[13]   N. C. George, K. A. Denault, R. Seshadri, *Annu. Rev. Mater. Res.* **2013** *43*, 481.

[14]   Z. Zhenrong, H. Xiang, L. Xu, *Appl. Optics* **2009**, *48*, 6627.

[15]   S. Wang, K. Wang, F. Chen, and S. Liu, *Opt. Express* **2011**, *19*, A716.

[16]   I. Moreno, *Optics Lett.* **2012**, *37*, 839.

[17]   S. L. Hsiao, N. C. Hu, H. Cornelissen, *Opt. Express* **2013**, *21*, A250.

[18]   C. C. Hsieh, Y. H. Li, C. C. Hung, *Appl. Optics* **2013**, *52*, 5221.

[19]   J. J. Wierer, A. David, M. M. Megens, *Nat. Photon.* **2009**, *3*, 163.

[20]   G. Lozano, D. J. Louwers, S. R. K. Rodriguez, S. Murai, O. T. A. Jansen, M. A. Verschuuren, J. Gómez Rivas, *Light: Sci. Appl.* **2013**, *2*, e66.

[21]   A. Polman, *Science* **2008**, *7*, 868.

[22]   P. Biagioni, J. S. Huang, B. Hecht, *Rep. Prog. Phys.* **2012**, *75*, 024402.

[23]   K. Okamoto, I. Niki, A. Shvartser, Y. Narukawa, T Mukai, A. Scherer, *Nat. Mater.* **2004**, 3, 601.

[24]   P. Anger, P. Bharadwaj, L. Novotny, *Phys. Rev. Lett.* **2006**, *96*, 113002.

[25]   S. Kühn, U. Hakanson, L. Rogobet, V. Sandoghdar, *Phys. Rev. Lett.* **2006**, *97*, 017402.

[26]   O. L. Muskens, V. Giannini, J. A. Sánchez-Gil, J. Gómez Rivas, *Nano Lett.* **2007**, *7*, 2871.

[27]   H. Iwase, D. Englund, J. Vučković, *Opt. Express* **2008**, *16*, 426.

[28]   A. Kinkhabwala, Z. Yu, S. Fan, Y. Avlasevich, K. Mullen, W. E. Moerner, *Nat. Photon.* **2009**, *3*, 654.

[29]   A. G. Curto, G. Volpe, T. H. Taminiau, M. P. Kreuzer, R. Quidant, N. F. van Hulst, *Science* **2010**, *329*, 930.

[30]   H. Aouani, O. Mahboub, E. Devaux, H. Rigneault, T. W. Ebbesen, J. Wenger, *Nano Lett.* **2011**, *11*, 2400.

[31]   L. Langguth, D. Punj, J. Wenger, A. F. Koenderink, *ACS Nano,* **2013**, *7*, 8840.

[32]   S. Murai, M. A. Verschuuren, G. Lozano, G. Pirruccio, S. R. K. Rodriguez, J. Gómez Rivas, *Opt. Express* **2013**, *21*, 4250.

[33]   F. J. García de Abajo, J. J. Sáenz, *Phys. Rev. Lett.* **2005**, *95*, 233901.

[34]   A. Christ, S. G. Tikhodeev, N. A. Gippius, J. Kuhl, and H. Giessen, *Phys. Rev. Lett.* **2003**, *91*, 183901.

[35]   F. J. García de Abajo. *Rev. Mod. Phys.* **2007**, *79*, 1267.

[36]   K. T. Carron, W. Fluhr, M. W. Meier, A. Wokaun, H. W. Lehman, *J. Opt. Soc. of Am. B* **1986**, *3*, 430.

[37]   B. Auguie, W. L. Barnes, *Phys. Rev. Lett.* **2008**, *101*, 143902.

[38]   V. G. Kravets, F. Schedin, A. N. Grigorenko, *Phys. Rev. Lett.* **2008**, *101*, 087403.

[39]   Y. Chu, E. Schonbrun, T. Yang, K. B. Crozier, *Appl. Phys. Lett.* **2008**, *93*, 181108.

[40]   G. Vecchi, V. Giannini, J. Gómez Rivas, *Phys. Rev. B* **2009**, *80*, 201401.

[41]   W. Zhou, T. W. Odom, *Nature Nanotech.* **2011**, *6*, 423.

[42]   G. Vecchi, V. Giannini, J. Gómez Rivas, *Phys. Rev. Lett.* **2009**, *102*, 146807.

[43]   V. Giannini, G. Vecchi, J. Gómez Rivas, *Phys. Rev. Lett.* **2010**, *105*, 266801.

[44]   S. R. K. Rodríguez, J. Gómez Rivas, *Opt. Express* **2013**, *21*, 27411.

[45]   A. I. Vakeväinen, R. J. Moerland, H. T. Rekola, A.-P. Eskelinen, J.-P. Martikainen, D.-H. Kim, P. Törma, *Nano Lett.* DOI**:** 10.1021/nl4035219.

[46]   W. Zhou, M. Dridi, J. Yong Suh, C. H. Kim, D. T. Co, M. R. Wasielewski, G. C. Schatz, T. W. Odom, *Nature Nanotechnol.* **2013**, *8*, 506.

[47]   S. Y. Chou, P. R. Krauss, P. J. Renstrom, *Appl. Phys. Lett.* **1996**, *67*, 3114.

[48]   L. J. Guo, *Adv. Mater.* **2007**, *19*, 495.

[49]   S. H. Ahn, L. J. Guo, *ACS Nano* **2009**, *3*, 2304.

[50]   R. Jia, M. Hornung, M. A. Verschuuren, R. van de Laar, J. van Eekelen, U. Plachetk, M. Moeller, C. Moormann, *Microelectron. Eng.* **2010**, *87*, 963.

[51]   F. Hua, Y. Sun, A. Gaur, M. A. Meitl, L. Bilhaut, L. Rotkina, J. Wang, P. Geil, M. Shim, John A. Rogers, A. Shim, *Nano Lett.* **2004**, *4*, 2467.

[52]   C. Peroz, S. Dhuey, M. Cornet, M. Vogler, D. Olynick, S. Cabrin, *Nanotechnology* **2012**, *23*, 015305.

[53]   G. Grzela, R. Paniagua-Domínguez, T. Barten, Y. Fontana, J. A. Sánchez-Gil, J. Gómez Rivas, *Nano Lett.* **2012**, *12*, 5481.

[54]   S. Zou, N. Janel, G. C. Schatz, *J. Chem. Phys.* **2004**, *120*, 10871.

[55]   M. Ringler, A. Schwemer, M. Wunderlich, A. Nichtl, K. Kurzinger, T. A. Klar, J. Feldmann, *Phys. Rev. Lett.* **2008**, *100*, 203002.

[56]   E. D. Palik, *Handbook of Optical Constants of Solids,* New York: Academic, **1985.**
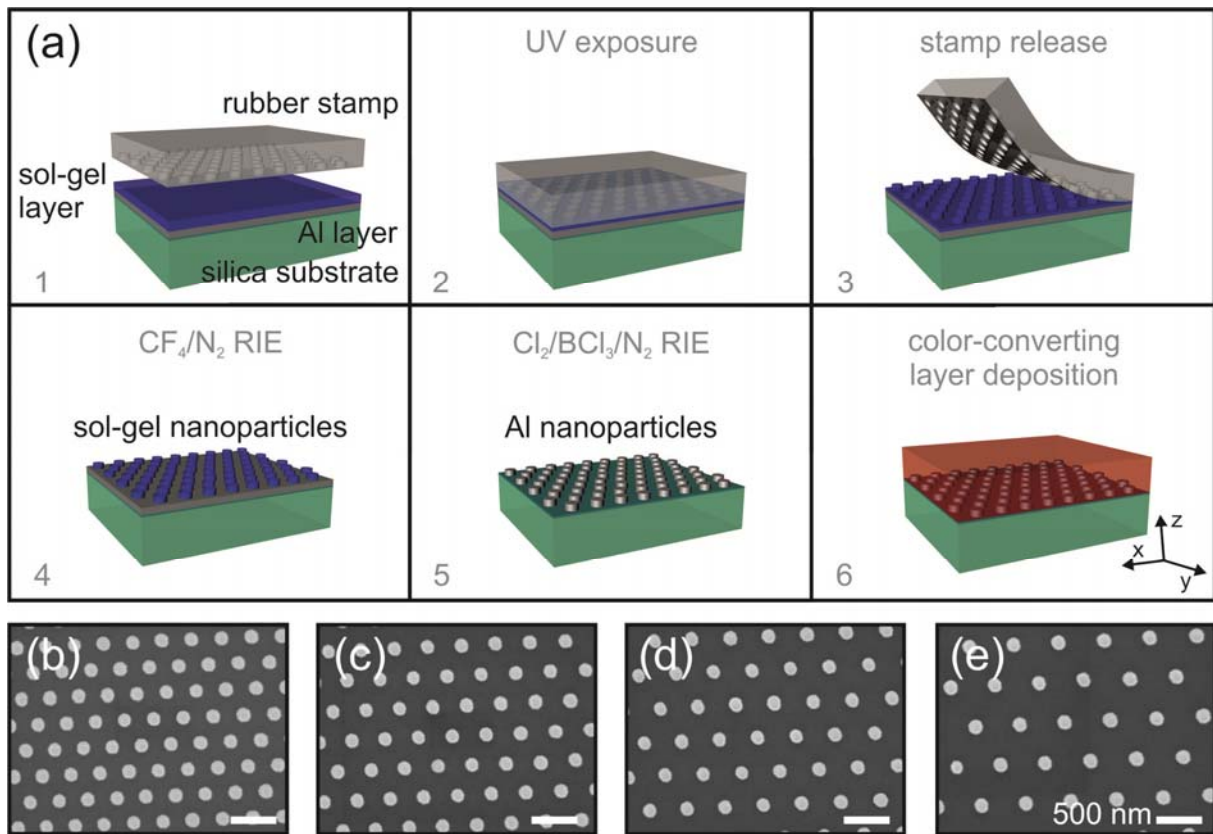
Figure 1. (a) Schematic of the fabrication process of the plasmonic-based color-converting layer. (b-e). Scanning electron microscope images of the top surface of the hexagonal array of Al nanoparticles deposited over a silica substrate. The lattice parameter of the array is (b) 325 nm, (c) 375 nm, (d) 425 nm and (e) 475 nm. The scale bars represent 500 nm.
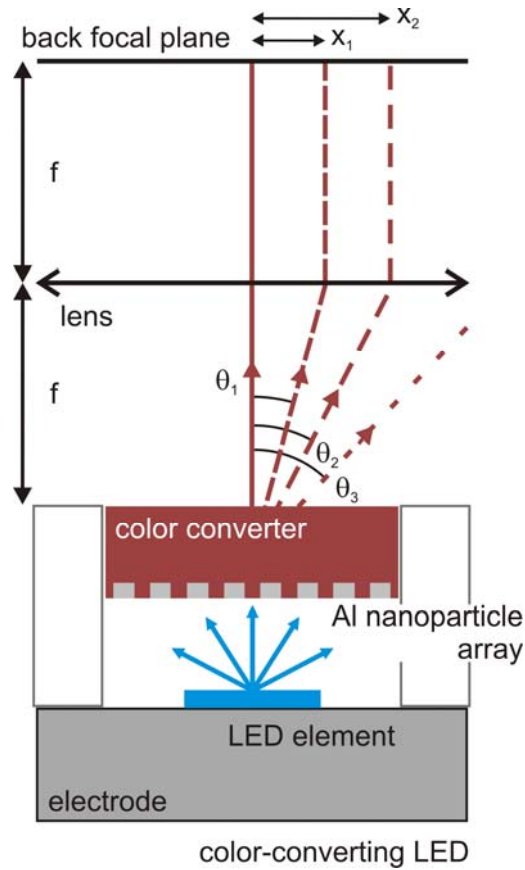
Figure 2. Schematic of the color-converting light emitting diode (LED). The upper part of the panel illustrates the working principle of Fourier microscopy. Light emitted by a color-converting LED at an angle θ_1 (θ_2) is collected at the position x_1 (x_2) in the back focal plane of the lens. Light emitted with an angle θ_3 is not picked up by the lens.
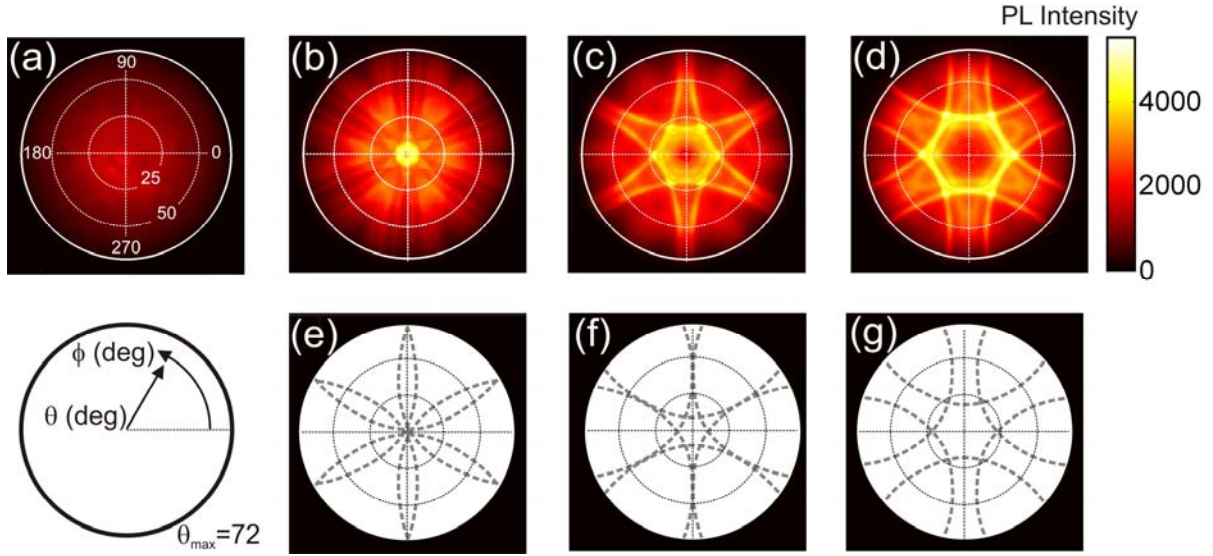
Figure 3. (a). Fourier image of the unpolarized emission from the non-plasmonic color converting layer, i.e. a 700 nm-thick dye-doped polymer layer deposited over a flat silica substrate. (c-d) Fourier images of the unpolarized emission of the same color-converting layer deposited over a hexagonal array of Al nanoparticles with lattice constant (b) a=475 nm, (c) a=425 nm and (d) a=375 nm. They are taken using a band pass filter with a central wavelength of 620 nm and a bandwith of 10 nm at full width at half maximum. An electrically-driven blue LED (λ_{ex}=445±15nm) is employed to optically excite the color-converting layer. The outermost circle indicates the maximum angle (θ_{max}=72 deg) that can be collected using an objective with a numerical aperture of 0.95. (e-f) Rayleigh anomalies (gray dashed curves) calculated for the (±1,0), (0, ±1), (-1,1) and (1,-1) beams diffracted by a hexagonal array with lattice constant (e) a=475 nm, (f) a=425 nm and (g) a=375 nm, in a medium with a refractive index of 1.46.
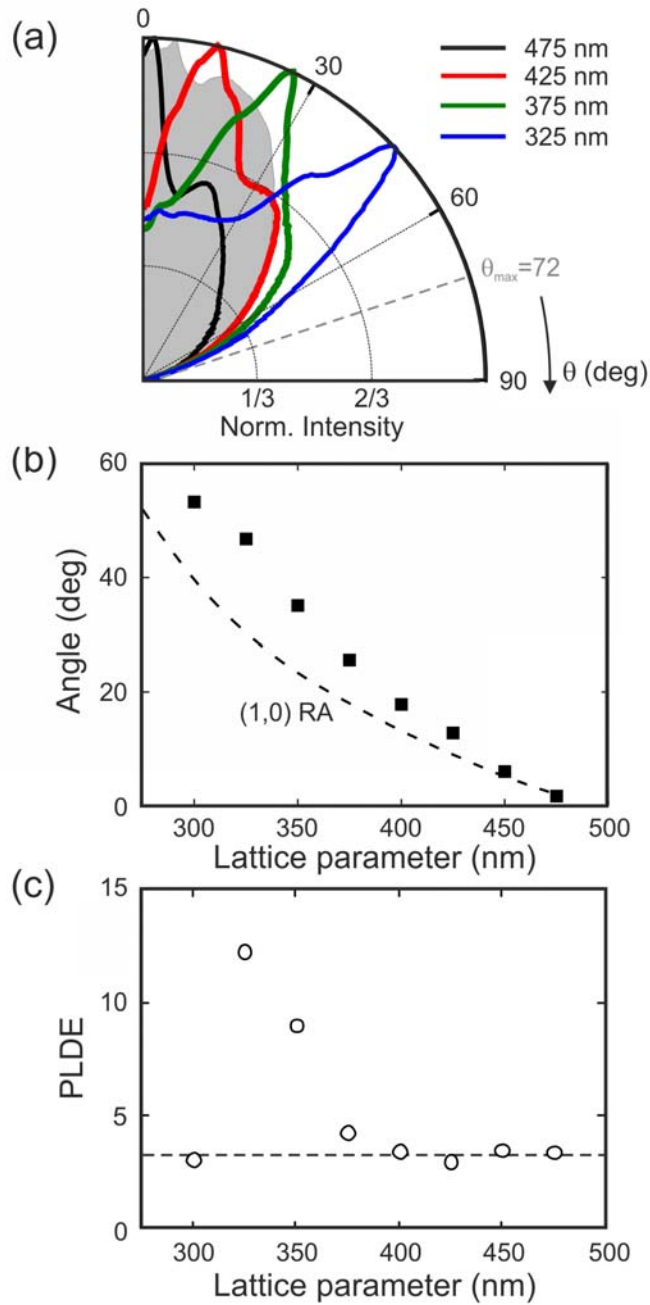
Figure 4. (a) Angular distribution of the unpolλarized emission (colored solid curves) in the wavelength range $\lambda=620\pm5$ from a 700 nm thick dye-doped polymer, acting as a color-converting layer, deposited over a hexagonal array of Al nanoparticles with lattice constant $a=475$ nm (black curve), $a=425$ nm (red curve), $a=375$ nm (green curve) and $a=325$ nm (blue curve). The grey filled area is the angular distribution of the unpolarized emission of the color-converting layer in the absence of the metallic nanoparticles. An electrically driven blue light emitting diode emitting at $\lambda_{ex}=445\pm15$ nm is employed to optically excite the color-

17

converting layer. Each radiation pattern is normalized to its maximum intensity. The dashed

gray line corresponds to the maximum angle (θ_{max}=72 deg) that can be collected in our setup.

(b) Emission angle at which most of the intensity is beamed as a function of the lattice

constant of the hexagonal array (black squares). Angular position of the Rayleigh anomaly

calculated for the (1,0) order diffracted by a hexagonal array as a function of the lattice

constant (dashed curve). (c) Photoluminescence directional enhancement (PLDE) defined as

the emission from the plasmonic color-converting layer at λ=620±5 nm normalized to the

emission of the color-converting layer on top of the flat silica substrate as a function of the

lattice constant of the hexagonal array. The dashed line is a guide to the eye.

The directional emission of color-converted light-emitting diodes (LEDs) can be enhanced and accurately controlled using nanoimprinted hexagonal arrays of aluminum nanoparticles. Such arrays sustain lattice-induced plasmonic-photonic modes, which are in spectral overlap with the emission of highly efficient dye molecules over narrow angular regions. The combination of large-area metal nanostructures fabricated by nanoimprint lithography and LEDs is beneficial for the design and optimization of solid-state lighting devices.

Light-emitting devices, nanophotonics, plasmonics, fluorescence, diffraction

G. Lozano*, G. Grzela, M. A. Verschuuren, and J. Gómez Rivas

Tailor-made directional emission in nanoimprinted plasmonic-based light-emitting devices

ToC figure